Mid-infrared radiation in an aperiodically poled $LiNbO_3$ superlattice induced by cascaded parametric processes

2004 J. Phys.: Condens. Matter 16 8465

(http://iopscience.iop.org/0953-8984/16/47/001)

INSTITUTE OF PHYSICS PUBLISHING JOURNAL OF PHYSICS: CONDENSED MATTER

J. Phys.: Condens. Matter **16** (2004) 8465–8474 PII: S0953-8984(04)85327-X

Mid-infrared radiation in an aperiodically poled $LiNbO_3$ superlattice induced by cascaded parametric processes

H C Guo[1], **Y Q Qin, Z X Shen and S H Tang**

Department of Physics, National University of Singapore, 117542, Singapore

E-mail: g0201826@nus.edu.sg (H C Guo)

Received 23 August 2004, in final form 21 October 2004
Published 12 November 2004
Online at stacks.iop.org/JPhysCM/16/8465
doi:10.1088/0953-8984/16/47/001

Abstract

The cascaded parametric processes, i.e. optical parametric oscillation (OPO) and difference frequency generation (DFG), can be used to induce efficient CW mid-infrared radiation at 4–5 μm in a single optical superlattice obtained by aperiodically poling a ferroelectric crystal. The superlattice consists of basic building blocks modulated by a spatial function. We numerically solve the coupling equations considering pump depletion and mid-IR absorption and realize the optimal condition for the cascaded frequency-down-conversion processes. Simultaneously, it is seen that the output performance is enhanced by the cascaded parametric design compared to the standard OPO configuration.

1. Introduction

Modulation of the third-order tensors (i.e. piezoelectric coefficients, electro-optical coefficients, and second-order optical susceptibilities) in the artificial superlattice materials, such as periodically poled $LiNbO_3$ (PPLN) [1], periodically poled $LiTaO_3$ (PPLT) [2], and periodically poled $KTiOPO_4$ (PPKTP) [3], can generate some interesting physical effects. For example, modulations of the piezoelectric coefficients and the electro-optical coefficients can result in ultrasonic excitation [4] and coupling between the extraordinary wave and ordinary wave [5], respectively. In the nonlinear optics field, the quasi-phase-matching (QPM) technique [6], which is achieved by offsetting the wavevector mismatch between the interacting waves via the reciprocal vectors of the superlattice, is the result of modulation of the nonlinear optical coefficients. The QPM technique is recognized to be more efficient than the conventional birefringent phase-matching method, but normally, a periodic optical superlattice (POSL) can effectively afford one reciprocal vector to compensate the mismatch

[1] Author to whom any correspondence should be addressed.

of the wavevectors in the optical parametric process. In fact, modulation of the nonlinear optical coefficients does not have to be restricted in a periodic structure; for example, a quasi-periodic [7] or aperiodic [8] one can afford more efficient reciprocal vectors, and thus cascaded optical parametric processes can be realized efficiently.

Recently, coherent mid-IR radiation in the 4–5 μm region has attracted much attention because of its potential applications in fundamental and applied scientific fields, including spectroscopy, chemical monitoring, environmental and atmospheric sensing, as well as biomedical and bioscience applications. However, tunable and high-power CW laser sources in this wavelength region are still in the development stage. Following advances in QPM techniques [9] and periodic poling processes [10], an OPO with PPLN was reported in 1995 [10]. Since then, the PPLN OPO has been extensively studied, both theoretically and experimentally, for CW operation in the infrared region of up to 4 μm [11–14]. While CW lasing in the 4–5 μm region of the mid-IR may be realized by extending the PPLN OPO design into this region, it is expected to be inherently low in efficiency because of the strong absorption by the ferroelectric crystal [14].

CW mid-IR generation with reasonable output power has been reported by combining the OPO and DFG processes in a single PPLN crystal [15]. This configuration circumvented the mid-IR absorption-high threshold problem which has curtailed the performance of CW PPLN OPO at wavelengths beyond 4 μm. However, as a unique reciprocal vector is used in this configuration to satisfy the QPM condition for both the OPO and the DFG processes, temperature tuning is additionally required to achieve quasi-phase-matching. Hence the design permits only a single mid-IR wavelength for a given specific temperature. The device stability is poor, as a small temperature fluctuation will disturb this stringent QPM condition. Furthermore, due to the fixed periodic structure, it does not have the flexibility to allow further adjustment to achieve optimal operating conditions.

In this paper, we propose an alternative scheme where QPM is achieved in an aperiodic optical superlattice (APOSL) comprising a single $LiNbO_3$ (LN) crystal. The design allows more than one predesigned reciprocal vector with a large Fourier coefficient to achieve cascaded interactions. Both the OPO and the DFG processes are phase matched simultaneously and coupled to each other throughout the entire length of the LN crystal, resulting in the efficient generation of both the mid-IR and idler waves. At the same time, since the APOSL allows greater variations in structural parameters, it is possible to adjust the domain sequence to attain the optimal condition for output power. As no additional temperature restriction is imposed, it can be easily extended to cover the entire mid-IR region of 4–5 μm. Furthermore, since both processes occur in a single crystal, the cavity configuration is compact and stable, and no additional alignments are required beyond those of a standard OPO.

2. Design of an APOSL for efficient cascaded mid-IR generation

2.1. QPM conditions and spatial function

It is seen that the trend in materials for nonlinear optics shows an ascending complexity from homogeneous crystals, POSL, quasi-periodic optical superlattice (QPOSL) [7] to APOSL [8]. Compared with POSL and QPOSL, the advantages of APOSL are threefold: more reciprocal vectors, flexibility over a wider range of wavelengths, and better uniformity in the Fourier coefficients of the reciprocal vectors. These considerations render the APOSL to be a truly viable design for cascaded mid-IR generation. The QPM conditions are:

$$\Delta k_{\mathrm{OPO}} = k_{\mathrm{p}} - k_{\mathrm{s}} - k_{\mathrm{i}} - G_{\mathrm{OPO}} = 0 \tag{1}$$

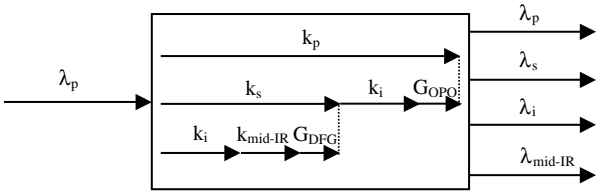

Figure 1. Schematic diagram of the cascaded process for efficient mid-IR generation in an APOSL. The APOSL has two predesigned reciprocal vectors G_{OPO} and G_{DFG} which are used to compensate the phase-mismatching for the OPO and the DFG processes respectively. Thus two QPM conditions are simultaneously achieved.

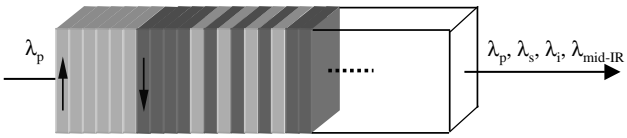

Figure 2. Schematic diagram shows an APOSL composed of building block d, modulated by the spatial function. The arrows indicate the directions of spontaneous polarization in ferroelectric materials.

for the OPO process and

$$\Delta k_{\mathrm{DFG}} = k_{\mathrm{s}} - k_{\mathrm{i}} - k_{\text{mid-IR}} - G_{\mathrm{DFG}} = 0 \tag{2}$$

for the DFG process, where k_{p}, k_{s}, k_{i}, $k_{\text{mid-IR}}$ represent the wavevectors of the pump, signal, idler, and mid-IR respectively. G_{OPO} and G_{DFG}, provided by the aperiodic structure, are the reciprocal vectors used to compensate the phase mismatching Δk_{OPO} and Δk_{DFG}. As shown in figure 1, the two coupled QPM processes, OPO and DFG, are simultaneously realized in a single superlattice. We consider for our case study a pump beam at 1.06 μm. The beam is first transformed into the signal and idler beams, followed by the generation of mid-IR in the 4–5 μm region along the entire length of the APOSL crystal.

The structural function of an APOSL is defined as [8]

$$S_{\mathrm{OPO+DFG}}(x) = H_{\Lambda_{\mathrm{DFG}}}(P) + \left[\mathrm{int}\left(\mathrm{int}\left(\frac{x}{d}\right)\tau\right) - \mathrm{int}\left(\left(\mathrm{int}\left(\frac{x}{d}\right)+1\right)\tau\right)\right] \times \left\{H_{\Lambda_{\mathrm{DFG}}}(P) - H_{\Lambda_{\mathrm{OPO}}}(P)\right\} \tag{3}$$

where $H_\Lambda(P)$ is defined as

$$H_\Lambda(P) = 1 - 2 \times \mathrm{int}\left(\frac{2P}{\Lambda}\right) + 4 \times \mathrm{int}\left(\frac{P}{\Lambda}\right) \tag{4}$$

and the variable P is given as

$$P = \frac{2 \times \mathrm{int}\left(\frac{x}{d}\right) + 1}{2} d. \tag{5}$$

$\mathrm{int}(x)$ takes the greatest integer $\leqslant x$, and Λ_{OPO} and Λ_{DFG} are the periods of the first-order periodic QPM structure. In equation (3), $\tau \in (0, 1)$ is a very important parameter, and it will be discussed in detail below. d is the length of the building block for the construction of the APOSL. The structural function $S_{\mathrm{OPO+DFG}}(x)$ only takes values +1 or −1, representing the two inverse polarization directions in ferroelectric materials. Figure 2 illustrates the schematic diagram of an APOSL defined by the structural function equation (3).

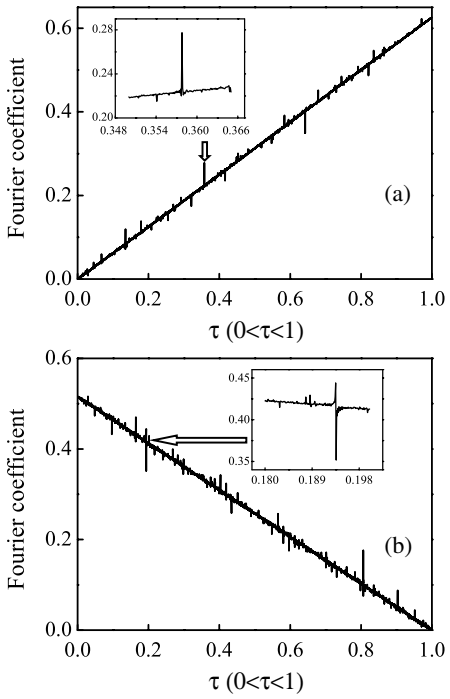

Figure 3. Relationship between the structural parameter τ of the APOSL and the Fourier coefficient. (a) As τ becomes larger, the Fourier coefficient of G_{OPO} increases with many local spike-like extrema. (b) As τ becomes larger, the Fourier coefficient of G_{DFG} decreases with many local spike-like extrema. The insets show one of the local extreme values.

As an example we consider the generation of mid-IR at 4.3 μm using the aforementioned CW pump beam at 1.06 μm. The LN crystal is chosen with a length of 50 mm. The wavelengths of the signal and the idler beams are set to be 1.7 and 2.8 μm respectively. As higher temperature is typically the case for CW operation as compared to pulsed PPLN OPO [11], we set the temperature to be 125 °C in our model. Using the LN dispersion relation and neglecting the thermal expansion, the structural parameters of the APOSL can be calculated from the Sellmeier equation [16] to be: $\Lambda_{\mathrm{OPO}} = 48.9\ \mu$m, $\Lambda_{\mathrm{DFG}} = 34.1\ \mu$m, $G_{\mathrm{OPO}} = 0.1285\ \mu\mathrm{m}^{-1}$ and $G_{\mathrm{DFG}} = 0.1843\ \mu\mathrm{m}^{-1}$.

2.2. Structural parameters d and τ

In the Fourier transform of the domain sequence as defined by the structural function, the magnitudes of the Fourier coefficients $g^{\mathrm{A}}_{\mathrm{OPO}}$ and $g^{\mathrm{A}}_{\mathrm{DFG}}$ ('A' for aperiodic) of the reciprocal vectors G_{OPO} and G_{DFG} are determined by the parameters d and τ. Normally $g^{\mathrm{A}}_{\mathrm{OPO}}$ and $g^{\mathrm{A}}_{\mathrm{DFG}}$ will increase as d becomes smaller [8]. However, in practice d is set to be 3.3 μm as limited by the poling process. The two Fourier coefficients are also closely related to τ. We have studied the relationship between the Fourier coefficients, $g^{\mathrm{A}}_{\mathrm{OPO}}$ and $g^{\mathrm{A}}_{\mathrm{DFG}}$, and the parameter τ by Fourier analysis. It is found that as τ grows, the magnitude of $g^{\mathrm{A}}_{\mathrm{OPO}}$ increases while the magnitude of $g^{\mathrm{A}}_{\mathrm{DFG}}$ decreases. Both of them have many local spike-like extrema, as shown in figure 3. In cascaded interactions, the photon energy is transferred from the pump beam to the signal beam and idler beam in the OPO process, and simultaneously from the signal beam to

Table 1. The values of the structural parameter τ and the relevant Fourier coefficients.

τ	0.3578	0.4087	0.4306	0.4311	0.4331	0.4346	0.4516	0.5274	0.5704
$g^{\mathrm{A}}_{\mathrm{OPO}}$	0.283	0.271	0.274	0.27	0.271	0.272	0.2824	0.331	0.351
$g^{\mathrm{A}}_{\mathrm{DFG}}$	0.33	0.326	0.294	0.295	0.298	0.294	0.303	0.252	0.2802

the idler beam and mid-IR beam in the DFG process. Therefore the coupling coefficients of these two nonlinear processes should be large enough to ensure a satisfactory generation of output power. Table 1 lists the selected values of $g^{\mathrm{A}}_{\mathrm{OPO}}$ and $g^{\mathrm{A}}_{\mathrm{DFG}}$ where both of them are set to be larger than 0.25.

3. Results and discussions

3.1. Coupling equations for the cascaded interactions and numerical solution

Under the small signal approximation (i.e. neglecting depletion) and ignoring losses, cascaded parametric interactions have been discussed in detail in QPOSL for the cases of cascaded third harmonic generation [17] and cascaded optical parametric generation [18]. However, under parametric oscillation at steady state, the pump depletion can be significant such that the small signal approximation is no longer tenable. In this section, we consider the cascaded parametric interactions with depletion and loss of mid-IR beam in the APOSL. In the cascaded interactions, the two nonlinear processes are coupled to each other in the entire length of the crystal. There are four waves, namely, the pump, signal, idler and mid-IR waves, propagating in the APOSL. Under the plane-wave approximation and the slowly varying envelope approximation and taking into consideration the absorption of the mid-IR wave and the QPM condition, the coupling equations that describe the cascaded interactions are given by

$$\begin{aligned}
\frac{\mathrm{d}E_{\mathrm{p}}}{\mathrm{d}x} &= \frac{-\mathrm{i}\omega_{\mathrm{p}} d_{\mathrm{eff}}}{n_{\mathrm{p}} c} g^{\mathrm{A}}_{\mathrm{OPO}} E_{\mathrm{s}} E_{\mathrm{i}} \\
\frac{\mathrm{d}E_{\mathrm{s}}}{\mathrm{d}x} &= \frac{-\mathrm{i}\omega_{\mathrm{s}} d_{\mathrm{eff}}}{n_{\mathrm{s}} c} \left(g^{\mathrm{A}}_{\mathrm{OPO}} E_{\mathrm{p}} E^{*}_{\mathrm{i}} + g^{\mathrm{A}}_{\mathrm{DFG}} E_{\mathrm{i}} E_{\text{mid-IR}} \right) \\
\frac{\mathrm{d}E_{\mathrm{i}}}{\mathrm{d}x} &= \frac{-\mathrm{i}\omega_{\mathrm{i}} d_{\mathrm{eff}}}{n_{\mathrm{i}} c} \left(g^{\mathrm{A}}_{\mathrm{OPO}} E_{\mathrm{p}} E^{*}_{\mathrm{s}} + g^{\mathrm{A}}_{\mathrm{DFG}} E_{\mathrm{s}} E^{*}_{\text{mid-IR}} \right) \\
\frac{\mathrm{d}E_{\text{mid-IR}}}{\mathrm{d}x} &= \frac{-\mathrm{i}\omega_{\text{mid-IR}} d_{\mathrm{eff}}}{n_{\text{mid-IR}} c} g^{\mathrm{A}}_{\mathrm{DFG}} E_{\mathrm{s}} E^{*}_{\mathrm{i}} - \frac{\alpha}{2} E_{\text{mid-IR}}
\end{aligned} \tag{6}$$

where $n_{\mathrm{p}}, n_{\mathrm{s}}, n_{\mathrm{i}}, n_{\text{mid-IR}}$; $\omega_{\mathrm{p}}, \omega_{\mathrm{s}}, \omega_{\mathrm{i}}, \omega_{\text{mid-IR}}$ represent the refractive index and angular frequency of the pump, signal, idler and mid-IR beams respectively. c is the speed of light in vacuum, d_{eff} is the second order nonlinear coefficient, and α is the absorption coefficient. Above the threshold, the signal beam oscillates as photon energy is being transferred from the pump beam to the signal and idler beams in the OPO process and simultaneously from the signal beam to the idler and mid-IR beams in the DFG process. Thus it is seen that both the idler and mid-IR beams are amplified during the cascaded interactions. As small signal approximation is no longer tenable and the two nonlinear processes are entangled all the time with mid-IR absorption, equation (6) can only be solved numerically. The calculation was carried out assuming no absorption of the signal and idler waves and no thermal dephasing. A linear optical cavity is chosen, and the mirror reflectivity for the signal wave is set to be 98%, and the transmission for the pump, idler, and mid-IR is set to be 100% for the two end mirrors. The signal field under the steady-state,condition is determined by the incident pump power,

the effective nonlinear coefficient, the crystal length, and the cavity loss, and is solved by numerical iteration followed by self-consistency.

3.2. Discussion of optimal condition for the cascaded interactions in the APOSL

The significant advantage of the cascaded APOSL design is that the optimal condition can be achieved by adjusting the structural parameter. As is known in cascaded interactions, the two nonlinear processes are entangled all the time and in the entire length of the crystal, and the energy distribution between them becomes more complex compared to the single parametric interaction. The essential factor in the cascaded parametric interactions is achieving the best trade-off between the energy distribution and the two nonlinear processes. Generation of mid-IR will suffer adversely if the pump beam is either not entirely converted to the signal and idler beams ('incomplete pump depletion') as shown in figure 4(a), or the pump beam is prematurely depleted and will drain energy from the signal and idler beams ('premature pump depletion') as shown in figure 4(b). The optimal condition for the cascaded mid-IR generation is complete pump depletion at the end of the crystal. The coupling coefficients, $g^{\mathrm{A}}_{\mathrm{OPO}}$ and $g^{\mathrm{A}}_{\mathrm{DFG}}$, involved in the coupling equations afford a powerful mechanism for achieving the optimal condition because they combine the energy distribution between the two nonlinear processes with the predesigned QPM structure, and hence the optimal condition does not have to rely on factors such as incident pump power, crystal length, and inherent material properties. One can obtain the optimal condition for any pump input and crystal length via the design of the QPM structure. As an example we analyse the optimal condition for the longest crystal (50 mm APOSL) and maximal pump input (CW 15 W) that are available for the present study. Fourier analysis shows that $g^{\mathrm{A}}_{\mathrm{OPO}}$ and $g^{\mathrm{A}}_{\mathrm{DFG}}$ are determined by the structural parameter τ, which is ultimately decided by the coupling equations. The simulation results show that seeking the largest Fourier coefficients for the two nonlinear processes does not necessarily correspond to the optimal output. In practice, $g^{\mathrm{A}}_{\mathrm{OPO}}$ has to be kept somewhat smaller than $g^{\mathrm{A}}_{\mathrm{DFG}}$, since mid-IR is generated essentially via the DFG process and a larger $g^{\mathrm{A}}_{\mathrm{OPO}}$ has a tendency to cause premature pump depletion. Of the values of τ listed in table 1, it is found that complete pump depletion at the end of the crystal occurs only when $\tau = 0.4087$, as shown in figure 4(c), which corresponds to $g^{\mathrm{A}}_{\mathrm{OPO}} = 0.271$ and $g^{\mathrm{A}}_{\mathrm{DFG}} = 0.326$ respectively, as shown in the Fourier spectrum (figure 5). Compared to figures 4(a) and (b), the output power increases by about 50% under the optimal condition.

The APOSL design shows good adaptability for analysing and achieving the optimal condition. We find that although the above optimal value of τ was analysed under 15 W incident pump power, it does not have to strictly rely on this input power. Actually this optimal value of τ can satisfy the optimal condition when the incident pump power changes in a finite range for a given superlattice length (our calculation shows the optimal value of τ obtained under 15 W pump input can fit the optimal condition in the 13–17 W range of pump power). It is beneficial to experimentally realize the optimal condition. The reason for this effect is that when the incident pump power varies, the circulating signal power should also change to satisfy self-consistency. Thus the photon energy distribution between the two nonlinear processes will be re-balanced, resulting in a re-achievement of the complete pump depletion at the end of the crystal under the same value of τ.

3.3. Output performance of cascaded APOSL design

In addition to optimal condition and better efficiency, the cascaded APOSL design has a more stable output power in comparison to the standard OPO configuration. In the standard OPO

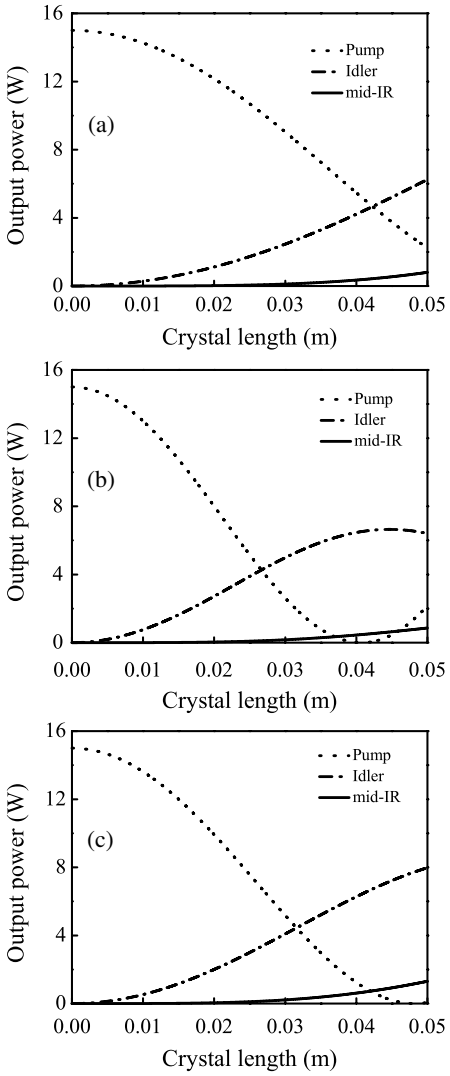

Figure 4. Photon flux trends of the pump, idler, and mid-IR waves in a 50 mm APOSL. (a) The pump wave is incompletely depleted, thus the energy transmission is inefficient. (b) The pump wave is prematurely depleted and will then grow at the expense of the signal and idler waves. The occurrence of both of these effects will slow down the growth rate of the mid-IR wave, although the growth is not blocked. (c) When $\tau = 0.4087$, optimal condition is achieved where the pump wave is completely depleted at the end of the crystal.

configuration, as the pump power increases, the idler beam (mid-IR beam) will reach an initial maximum only to be followed by a draining off of energy by the depleted pump, while for the cascaded APOSL design, equation (6) infers that mid-IR is only indirectly related to the pump via the DFG process. Thus a complete pump depletion does not immediately lead to a drop of the mid-IR output. Actually, in the cascaded APOSL design, the two nonlinear processes are coupled to each other in the entire crystal, and both of the idler and mid-IR waves are amplified via the cascaded interactions. As shown in figure 6, for the standard OPO configuration (dashed curve), the mid-IR output power reaches a maximum of about 1.5 W for $P_{\text{pump}} \approx 9$ W. As

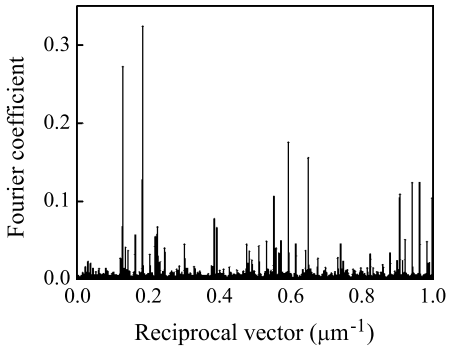

Figure 5. Fourier spectrum of the aperiodic spatial function equation (3) when τ equals 0.4087.

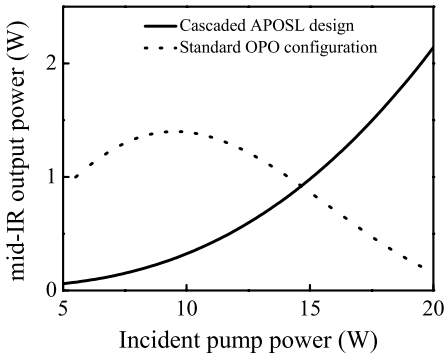

Figure 6. The mid-IR output power versus the different incident pump power. The dashed curve is for the standard OPO configuration and the solid curve is for the cascaded APOSL design. The mid-IR output power in the cascaded APOSL design continuously increases in a wider pump variation range, resulting in enhanced stability, and higher power mid-IR generation is ultimately ensured compared to the standard OPO configuration.

(This figure is in colour only in the electronic version)

the input pump power increases to 20 W, the mid-IR output severely decreases, while for the cascaded APOSL design (solid curve), the mid-IR power grows continuously to about 2.2 W when the pump power increases to the same value. It is seen that by using the new cascaded APOSL design, higher power mid-IR generation is achieved in a wider range of pump power.

On the other hand, in the standard OPO configuration maximal mid-IR output can only be obtained for a fixed incident pump power (denoted as $P_{\text{pump-fix}}$) for a given crystal length and cavity loss. Any experimental uncertainty such as the non-ideal nature of the domain inversion, a variation of the superlattice length during the poling process, the fluctuation of the cavity and the pump source, will cause this predesigned $P_{\text{pump-fix}}$ to deviate from the actual value and destabilize the operation with a severe drop of the mid-IR output, as depicted by the dashed curve in figure 6, whereas for the cascaded APOSL design, this severe deviation can be circumnavigated because the design accepts a wider range of pump power, as depicted by the solid curve in figure 6. Therefore enhanced device stability is obtained in the cascaded APOSL design.

Due to the narrow acceptance bandwidth of the QPM DFG [19], almost all the other operating points reachable by temperature tuning are beyond the acceptance bandwidth of the

Table 2. Structural parameters of the multiple-grating APOSL for the tuning.

Wavelength (μm)	4.1	4.2	4.3	4.4	4.6	4.7	4.9
d (μm)	3.3	3.3	3.3	3.3	3.3	3.3	3.3
τ	0.4760	0.4555	0.4087	0.4605	0.4371	0.5546	0.4885
$g^{\mathrm{A}}_{\mathrm{OPO}}$	0.323	0.302	0.271	0.282	0.269	0.293	0.297
$g^{\mathrm{A}}_{\mathrm{DFG}}$	0.332	0.331	0.326	0.322	0.317	0.318	0.323

DFG process, resulting in inherently poor temperature tunability. Realization of wavelength tuning in the OPO-DFG configuration has to be combined with a multiple-grating approach. Fortunately the two nonlinear processes are coupled in the single crystal at all times in the cascaded APOSL design, thus wide tuning is achieved by a multiple-grating approach without having to sacrifice cavity simplicity as compared to other configurations [20]. In table 2, we list the structure parameters for multi-grating tuning.

Finally, the idler wave in the cascaded APOSL design, fuelled by the OPO and the DFG processes, also grows steadily and produces a high efficiency idler beam output. In other words, both efficient mid-IR and idler generations can be realized, making this design practical for the construction of IR to mid-IR generators.

4. Conclusions

In summary, we have designed and analysed the cascaded mid-IR (4–5 μm region) generation using an APOSL design. Cascaded parametric interactions between the OPO and DFG processes for frequency-down-conversion is investigated from a new perspective. The coupling equations are solved numerically, and the optimal condition is discussed and realized by adjusting the structural parameters of the APOSL. High power generation is ensured since the two nonlinear processes are coupled in the entire length of the crystal and the mid-IR beam experiences nonlinear gain continuously throughout the crystal. The cascaded APOSL design has improved stability when the incident pump power varies over a wide range, making it more suitable for high power operation as compared to the standard OPO configuration. Besides mid-IR, the idler beam is amplified at the same time via the two nonlinear processes in the entire length of the crystal, and can be extracted for output. By adjusting the structural parameter of the APOSL in a multiple grating design, a wide tuning range can be achieved with the compact cavity design. The results presented here offer flexibility in the design of a CW tunable, all-solid, compact, high-power IR to mid-IR (4–5 μm) generator.

Acknowledgment

This work is supported by the DSTA of Singapore under Grant No. POD0103451.

References

[1] Yamada M, Nada N, Saitoh M and Watanabe K 1993 *Appl. Phys. Lett.* **62** 435
[2] Zhu S-N, Zhu Y-Y, Zhang Z-Y, Shu H and Wang H-F 1995 *J. Appl. Phys.* **77** 5481
[3] Risk W P and Lau S D 1996 *Appl. Phys. Lett.* **69** 3999
[4] Zhu Y Y and Ming N B 1992 *J. Appl. Phys.* **72** 904
[5] Lu Y Q, Wang Z L, Wang Q, Xi Y X and Ming N B 2000 *Appl. Phys. Lett.* **77** 3719
[6] Armstrong J A, Bloembergen N, Ducuing J and Pershan P S 1962 *Phys. Rev.* **127** 1918
[7] Qin Y-Q, Su H and Tang S-H 2003 *Appl. Phys. Lett.* **83** 1071

[8] Liu H, Zhu Y Y, Zhu S N, Zhang C and Ming N B 2001 *Appl. Phys. Lett.* **79** 728
[9] Fejer M M, Magel G A, Jundt D H and Byer R L 1992 *IEEE J. Quantum Electron.* **28** 2631
[10] Myers L E, Eckardt R C, Fejer M M, Byer R L, Bosenberg W R and Pierce J W 1995 *J. Opt. Soc. Am.* B **12** 2102
[11] Myers L E and Bosenberg W R 1997 *IEEE J. Quantum Electron.* **33** 1663
[12] Powers P E, Kulp T J and Bisson S E 1998 *Opt. Lett.* **23** 159
[13] Stothard D J M, Ebrahimzadeh M and Dunn M H 1998 *Opt. Lett.* **23** 1895
[14] Myers L E, Eckardt R C, Fejer M M, Byer R L and Bosenberg W R 1996 *Opt. Lett.* **21** 591
[15] Chen D-W and Masters K 2001 *Opt. Lett.* **26** 25
[16] Jundt D H 1997 *Opt. Lett.* **22** 1553
[17] Zhu S-N, Zhu Y-Y and Ming N-B 1997 *Science* **278** 843
[18] Du Y, Zhu S N, Zhu Y Y, Xu P, Zhang C, Chen Y B, Liu Z W, Ming N B, Zhang X R, Zhang F F and Zhang S Y 2002 *Appl. Phys. Lett.* **81** 1573
[19] Liu X, Zhang H and Guo Y 2001 *J. Lightwave Technol.* **19** 1785
[20] Chen D-W 2003 *J. Opt. Soc. Am.* B **20** 1527